

Effect of temperature on crack kinking and jumping in a cross-ply laminated beam

S. YAMAMOTO¹⁾, T. IKEDA¹⁾, A. SENBA²⁾

¹⁾*Department of Aerospace Engineering
Nagoya University
Furo-cho, Chikusa-ku
Nagoya 464-8603, Japan
e-mail: ikeda@nuae.nagoya-u.ac.jp*

²⁾*Department of Vehicle and Mechanical Engineering
Meijo University
1-501 Shiogamaguchi, Tenpaku-ku
Nagoya 468-8502, Japan
e-mail: senba@meijo-u.ac.jp*

TO UNDERSTAND THE MECHANISMS of crack kinking and jumping that occur within the 90° layer of a cross-ply fiber reinforced plastic laminated plate, double cantilever beam tests were performed at several temperatures for laminated plates with two types of stacking sequences. The crack kink angles were calculated using a bi-layer shear-deformable beam model. Furthermore, the interlaminar shear stresses were calculated using finite-element models to clarify the mechanism of the repeated jumps. The following results were obtained from these experiment and analysis; (i) a crack at the center tended to propagate in a self-similar manner more stably at higher temperatures, (ii) the applied load at which value the crack at the center started propagation decreased as the 90° layer became thicker, and (iii) the crack along a $0^\circ/90^\circ$ interface jumped to the other interface because the shear force along the $0^\circ/90^\circ$ interface due to the thermal stress decreased as the crack propagated along the interface.

Key words: laminated plate, crack propagation, crack kinking, crack jump, thermal stress, analytical modeling.

Copyright © 2016 by IPPT PAN

1. Introduction

CARBON FIBER REINFORCED PLASTIC (CFRP) has become one of the primary materials used in the aerospace industry in recent years because of its high specific strength and stiffness. However, its low interlaminar strength may lead to delamination, the propagation of which can cause structural failure. Therefore, it is important for structural designers to be able to characterize delamination resistance. One way to do this is with the double cantilever beam (DCB) test that was established for unidirectional laminates. However, multidirectional lam-

inates such as quasi-isotropic ones composed of 0° , 45° , -45° , and 90° plies are used in most applications of CFRP structures. Accordingly, several studies have been conducted concerning the effects of ply orientation on the propagation mode [1–7]. However, it has been shown that measuring the interlaminar fracture toughness of multidirectional laminates is difficult because the delamination does not propagate in a self-similar manner between layers. Rather, cracks tend to kink and jump to interfaces [1]. For example, consider the DCB test of a cross-ply CFRP laminate with a stacking sequence of $[90_m^\circ/0_n^\circ/90_m^\circ//90_m^\circ/0_n^\circ/90_m^\circ]$, where “//” represents the initial position of a crack. An initial crack can kink toward one of the $0^\circ/90^\circ$ interfaces and reach it. After the crack has propagated a short distance along this interface, it will occasionally jump to the other $0^\circ/90^\circ$ interface. In this paper, crack kinking means that an initial crack has deviated from the line of its initial direction or that a crack that was propagating along an interface has deviated from it. Crack jumping means that after kinking, a crack has propagated and reached an interface.

Various techniques have been proposed to avoid crack kinking and jumping. HUNSTON and BASCOM [1] suggested using some 0° plies in the planes adjacent to the delamination one. ROBINSON and SONG [2] proposed a DCB specimen with pre-delaminated edges to avoid intralaminar damage. However, it is now known that monitoring crack positions is difficult and that intralaminar damage is not always avoided [4–5]. SEBAEY *et al.* [6] investigated the probability of a crack jump occurring during a DCB test and showed that it is inversely related to the arm-bending stiffness. The interlaminar and intralaminar energy release rates were calculated by de MORAIS *et al.* [7] using finite-element models combined with the virtual crack closure technique (VCCT) in which the crack propagation paths were assumed. Their results showed that the intralaminar energy release rate is significantly smaller than the interlaminar one. This suggested that the intralaminar crack propagation, that is the crack jumping, is unavoidable in tough multidirectional laminates.

Some researchers have considered the effects of the residual thermal stress that results from the difference between the cure and test temperatures. DE MORAIS *et al.* [7] concluded that thermally induced stresses can be neglected when considering fracture toughness. NAIRN [8] showed that the mode I fracture toughness is highly dependent upon the thermal stresses. SEBAEY *et al.* [6] demonstrated that the induced thermal stresses affect the probability of crack jumping; they have no effect on the load–displacement curves.

RATCLIFFE *et al.* developed a new test method of investigating crack kinking and jumping. This method is based on a clamped-beam configuration that has $0^\circ/90^\circ$ and $90^\circ/0^\circ$ interfaces [9–11] or $0^\circ/\theta$ and $\theta/0^\circ$ ones in which $\theta = 60^\circ$ or 75° [12]. They assumed that the sign of the interlaminar shear stress affects the direction of a kink. Numerical simulations using the VCCT and the floating-node

method (FNM) corroborated this assumption [9] and reproduced the overall failure morphology that was observed experimentally [11]. In their tests, single jump events occurred, but the repeated jumps that are observed in DCB tests did not.

However, there have been only a few studies on crack propagation and kink angle in cross-ply DCB specimens. Being able to predict complex fracture behaviors in which interlaminar and intralaminar fractures occur would help to improve the precision of CFRP structural design.

Some analysis of crack kinking in DCB tests of foam core sandwich beams has been performed. CARLSSON *et al.* [13] used a finite-element method to predict the kink angle in such tests. YOKOZEKI [14] used an analytical formulation of the rate of energy release from the foam core to predict the kink angle and to examine the effect of the residual thermal stress due to the difference between the cure and test temperatures. He concluded that this method is capable of predicting the locations of steady-state cracks in sandwich beams. The applied load must be specified if residual thermal stress is included in the kink-angle calculation; it is not required otherwise. In this study, a 1 N load was used to examine the effect of residual thermal stress.

The complex fracture behaviors of multidirectional laminates, which include interlaminar and intralaminar fractures, were analyzed in this investigation for cross-ply DCB specimens in particular. Although DCB tests were carried out, the primary aim was not to measure the critical energy release rate in mode I G_{IC} of the specimens. Firstly, DCB tests of cross-ply laminates were conducted at various temperatures to determine the crack propagation behaviors of cross-ply DCB specimens and its temperature dependence. Then, by applying Yokozeki's analytical formulation [14] to the cross-ply DCB specimens and specifying an adequate applied load, crack propagation was predicted analytically. This was done to understand the mechanisms of crack kinking and jumping and for comparison with the experimental results for cross-ply CFRP laminates. The effect of the test temperature on the crack propagation path was also examined.

The motivation for using cross-ply laminates in this study was that although composite structures are rarely built using cross-ply laminates alone, these structures often contain regions in which such materials dominate. Moreover, cross-ply laminates are relatively simple and yet encapsulate the essential mechanical behaviors of multi-directional ones.

2. Experiment

2.1. Specimens

We considered cross-ply CFRP laminates with a stacking sequence of $[90^{\circ}_m/0^{\circ}_n/90^{\circ}_m//90^{\circ}_m/0^{\circ}_n/90^{\circ}_m]$, where again “//” represents the initial po-

sition of a crack. The laminated plates used in this study were made of unidirectional pre-impregnated (prepreg) sheets (TR380G-250SM, Mitsubishi Rayon Inc.). Those with $(m, n) = (2, 4)$ are referred to as Type A and those with $(m, n) = (1, 6)$ as Type B. The initial cracks were made by inserting 12.5 μm polytetrafluoroethylene (PTFE) films between the 90° plies. The cure cycle is shown in Fig. 1; the specimens were cured at 130°C for 90 min. A schematic diagram of the DCB test and the dimensions of the DCB specimen is shown in Fig. 2. P , δ , and a denote the applied load, displacement, and crack length, respectively; the initial crack length was 54 mm.

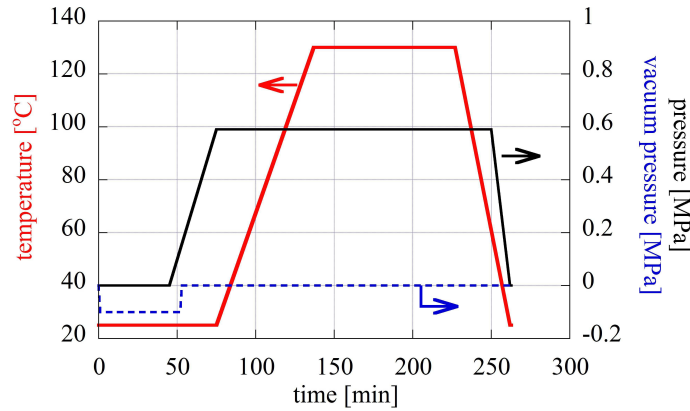


FIG. 1. Cure cycle.

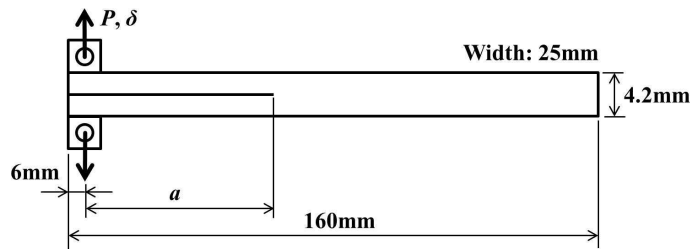


FIG. 2. Schematic of DCB test specimen.

2.2. Test procedures

The test procedures followed a standard method (Japanese Industrial Standard, JIS K 7086 [15]). All of the tests were carried out under displacement control by a biaxial servo-hydraulic machine (Type 8850, Instron) at an actuator speed of 0.5 mm/min. The DCB tests were performed at six temperatures ($-25, 0, 25, 50, 75,$ and 100°C), and three different specimens were tested at each

temperature. In these tests, no pre-cracks were made before the tests because such cracks tend to kink toward one of the $0^\circ/90^\circ$ interfaces. Load–displacement curves were recorded during loading, and a microscope (VHX-600, Keyence) was used to inspect both sides of each specimen after the tests.

2.3. Results

Typical load–displacement curves are shown in Fig. 3 for each temperature. It can be seen that shapes of these curves depend on the test temperature. The initial slope of Type B is larger than that of Type A because the former includes more 0° layers and is stiffer than the latter. The compliance increases in both types after the large load drop.

Typical crack propagation paths for Type A and Type B specimens are shown in Figs. 4 and 5, respectively, at each temperature. In Type A specimens at $<50^\circ\text{C}$, the initial cracks kinked almost vertically upward or downward. After they reached $0^\circ/90^\circ$ interfaces, the cracks propagated along the interfaces. However, at 75°C , the crack jumped to the other interface after propagating a short distance along the $0^\circ/90^\circ$ interface. At 100°C , the crack propagated in an almost self-similar manner a short distance from the center of the specimen and kinked toward the interface. After the crack reached the interface and propagated a short distance along the interface, it kinked and proceeded to the center of the specimen.

The magnitudes of the initial crack kink angle defined in Fig. 6 are listed in Table 1, where it can be seen that this angle decreased as the test temperature was raised. Clearly, crack propagation path is heavily dependent on the test temperature.

Table 1. Magnitudes of initial crack kink angle.

Temp. [$^\circ\text{C}$]		–25	0	25	50	75
Magnitude of initial crack kink angle [$^\circ$]	Type A	83 ± 6	81 ± 5	79 ± 5	72 ± 9	62 ± 4
	Type B	74 ± 4	67 ± 2	57 ± 4	48 ± 4	–

In each Type B specimen at -25°C , the crack kinked toward one of the $0^\circ/90^\circ$ interfaces and propagated along the interface upon reaching it. At 0, 25, and 50°C , the cracks jumped to the other interfaces after propagating short distances along the $0^\circ/90^\circ$ interfaces. The cracks jumped repeatedly in these cases. The intervals between the crack jumps are listed in Table 2, where Δa_1 and Δa_2 are defined as the distances from the initial crack tip to the first and second crack kinking points, respectively, as shown in Fig. 6. It can be seen from Table 2 that the intervals between the crack jumps became shorter as the test temperature was increased. The crack kink angles decreased as the test

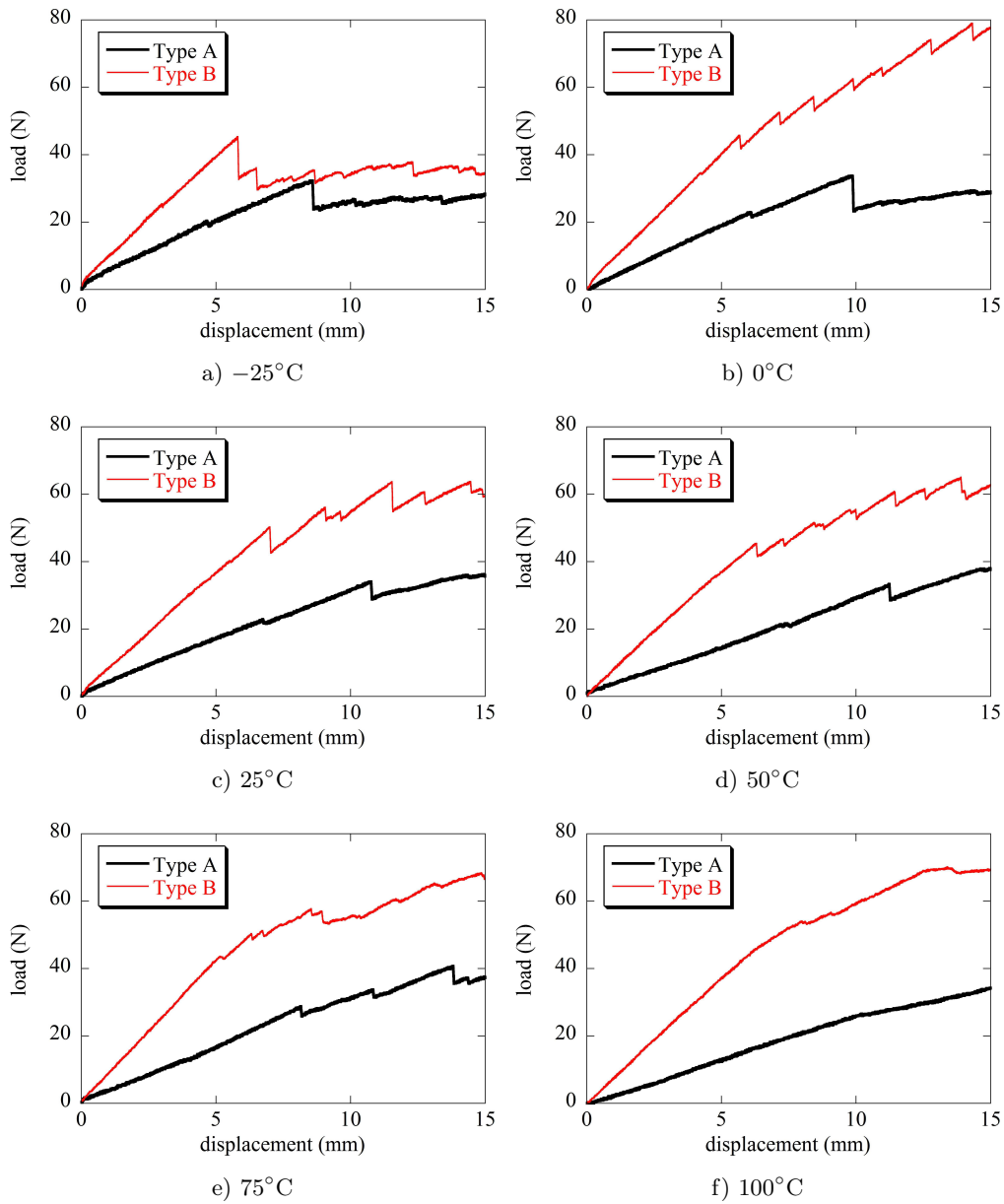


FIG. 3. Typical load–displacement curves.

temperature was raised, as shown in Table 1. At 75°C and 100°C, the cracks propagated in an almost self-similar manner near the centers of the specimens.

In both types of specimens, secondary cracks were observed sometimes at the initial crack tips, which kinked almost symmetrically to the primary cracks

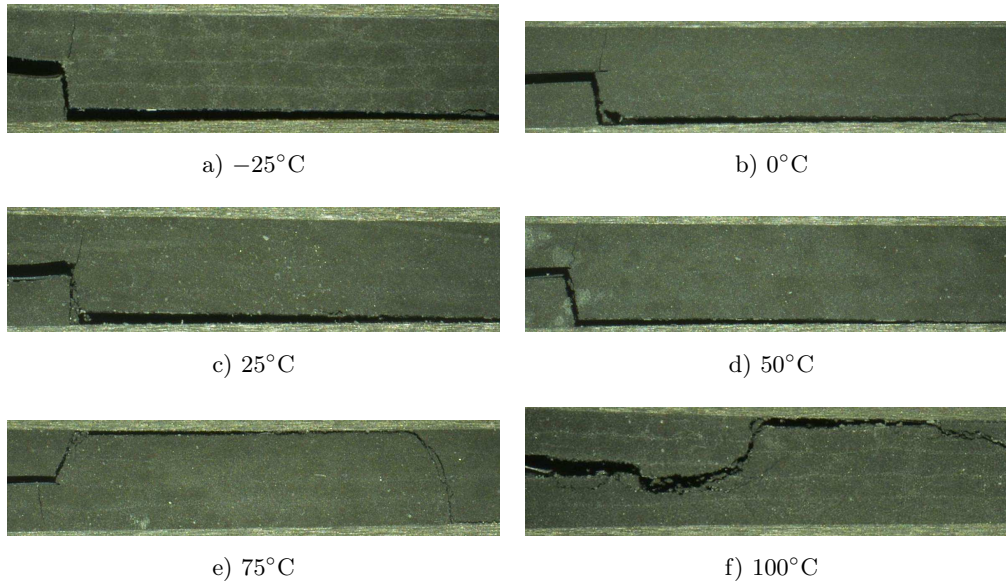


FIG. 4. Crack propagation path for Type A specimens with a stacking sequence of $[90^{\circ}_2/0^{\circ}_4/90^{\circ}_2//90^{\circ}_2/0^{\circ}_4/90^{\circ}_2]$.

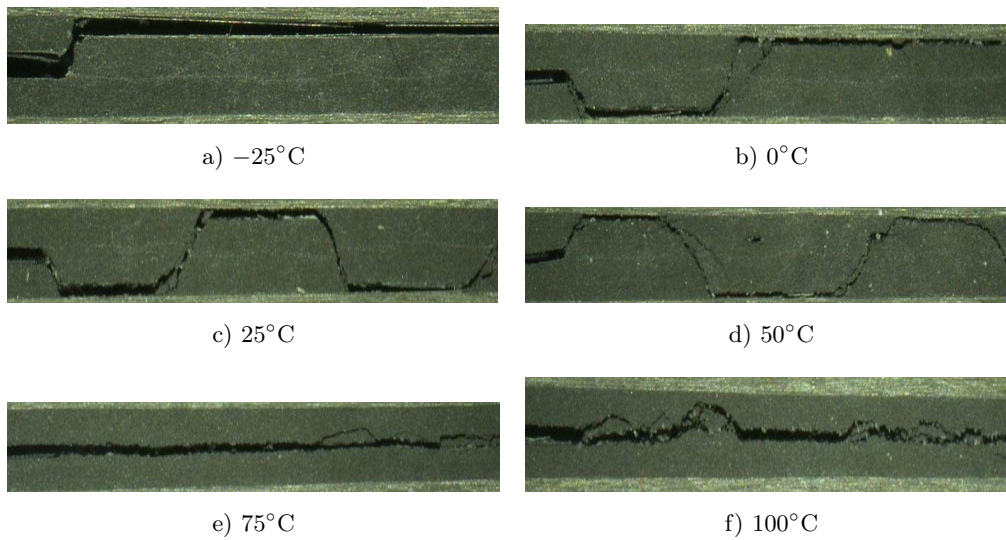


FIG. 5. Crack propagation paths for Type B specimens with a stacking sequence of $[90^{\circ}/0^{\circ}_6/90^{\circ}//90^{\circ}/0^{\circ}_6/90^{\circ}]$.

as shown in Fig. 7. We think that these secondary cracks occurred because of a longitudinal tensile stress due to flexure in the same manner as primary cracks

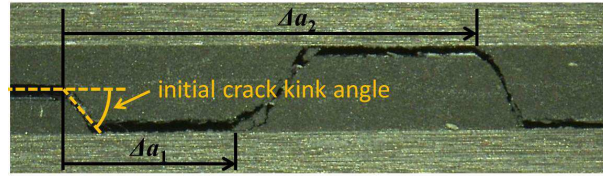


FIG. 6. Definitions of initial crack kink angle and distance from initial crack tip to crack kinking points.

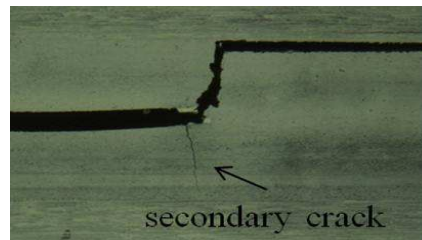


FIG. 7. Secondary crack at initial crack tip in Type-A specimen.

Table 2. Distances of crack kinking points from initial crack tips.

Type	Temp. [°C]	Δa_1 [mm]	Δa_2 [mm]
A	75	3.4 ± 0.8	7.0 ± 0.6
B	0	1.9 ± 0.3	5.2 ± 1.2
	25	1.5 ± 0.5	3.0 ± 0.5
	50	1.4 ± 0.4	2.8 ± 0.4

occur. This is because the same bending stress occurs at both the upper and lower legs in the DCB tests. Therefore, we consider that the initial crack kinking occurred because of the flexure fracture.

In the cases in which the crack jumped repeatedly, it can be seen in Figs. 3–5 that the load increased beyond the value before it dropped as the displacement increased. However, in most of the cases in which the crack propagated along an interface only after reaching it by means of kinking toward it, the load did not increase beyond the value before it dropped.

3. Analysis of crack kinking

YOKOZEKI [16] derived the energy release rates of delaminated multilayered materials based on a bi-layer shear-deformable beam model that included resid-

ual thermal stress. He applied this formulation to foam core sandwich beams and concluded that this method is capable of predicting both crack kink angles and steady-state crack locations [14]. This analytical formulation was applied here to cross-ply laminates to predict their crack kinking behaviors and to compare the predicted results with the experimental ones.

3.1. Energy release rate and crack kink angle

This section summarizes Yokozeki's energy release rate formulation [14, 16] based on a simple bi-layer shear-deformable beam model and its application to crack kinking analysis.

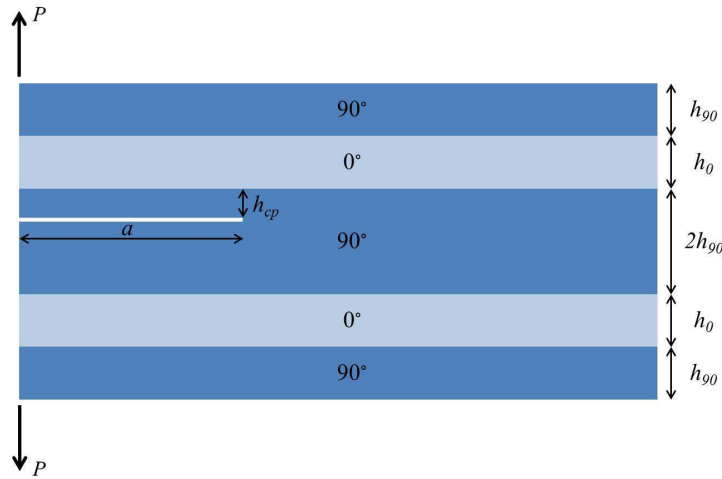


FIG. 8. Schematic of DCB cross-ply specimen.

A schematic of a cross-ply laminate with a crack of length a is shown in Fig. 8. The system is assumed to be a bi-layer shear-deformable beam with concentrated shear and normal forces at the crack tip, as presented in Fig. 9. It is assumed that the cracked arms are separated and that any contact between the crack surfaces can be neglected. The shear force Q_c and the normal tensile force N_c at the crack tip can be expressed by considering the force balance as

$$(3.1) \quad Q_c = \frac{2(M\xi - N\eta)}{h_1\xi + 2\eta},$$

$$(3.2) \quad N_c = -Q - \lambda \left(M + \frac{h_1}{2} N \right),$$

$$\begin{aligned}
 (3.4) \quad \beta &= \left(b_1 + b_2 + \frac{h_1 + h_2}{2} d_2 \right) \xi + (d_1 + d_2) \eta, \\
 \chi &= \left(\frac{1}{\kappa C_1} + \frac{1}{\kappa C_2} \right) \left(a_1 + a_2 - h_1 b_1 + h_2 b_2 + \frac{h_1^2}{4} d_1 + \frac{h_2^2}{4} d_2 \right), \\
 \begin{bmatrix} a_i & b_i \\ b_i & d_i \end{bmatrix} &= \begin{bmatrix} A_i & B_i \\ B_i & D_i \end{bmatrix}^{-1}, \quad \begin{Bmatrix} \alpha_{Ni} \\ \alpha_{Mi} \end{Bmatrix} = \begin{bmatrix} a_i & b_i \\ b_i & d_i \end{bmatrix} \begin{Bmatrix} N_{Ti} \\ M_{Ti} \end{Bmatrix}, \quad C_i = B \int G_i dz_i, \\
 A_i &= B \int E_i dz_i, \quad B_i = B \int E_i z_i dz_i, \quad D_i = B \int E_i z_i^2 dz_i, \\
 N_{Ti} &= B \int E_i \alpha_i \Delta T dz_i, \quad M_{Ti} = B \int E_i \alpha_i \Delta T z_i dz_i.
 \end{aligned}$$

The parameters h_0 , h_{90} , and h_{cp} are, respectively, the thicknesses of the 90° and 0° layers and the distance between the upper $0^\circ/90^\circ$ interface and the initial crack position defined in Fig. 8. B and ΔT denote the width of the beam and the temperature difference between the cure and test temperatures, respectively. The local coordinates x_i and z_i and the global coordinate x are defined in Fig. 9. The subscript i denotes each sublaminar, and E , G , and α denote Young's modulus, the shear modulus, and the linear expansion coefficient, respectively. κ is the shear factor, which was assumed to be $5/6$ for the rectangular cross section in this study.

The energy release rates G_I and G_{II} can be calculated in terms of the crack tip forces as

$$(3.5) \quad G_I = \frac{1}{2B} \left(\frac{1}{\kappa C_1} + \frac{1}{\kappa C_2} \right) N_c^2$$

and

$$(3.6) \quad G_{II} = \frac{1}{2B} \left(a_1 + a_2 - h_1 b_1 + h_2 b_2 + \frac{h_1^2}{4} d_1 + \frac{h_2^2}{4} d_2 \right) Q_c^2.$$

In this study, the 90° ply was assumed to be an isotropic homogeneous material. Therefore, the stress intensity factors could be determined from the energy release rates by using the following formulae:

$$(3.7) \quad K_I = \begin{cases} \sqrt{E_T G_I} & (N_c > 0), \\ -\sqrt{E_T G_I} & (N_c < 0), \end{cases}$$

and

$$(3.8) \quad K_{II} = \begin{cases} \sqrt{E_T G_{II}} & (Q_c > 0), \\ -\sqrt{E_T G_{II}} & (Q_c < 0). \end{cases}$$

Here, E_T denotes the Young's modulus of the 90° ply. The signs of the stress intensity factors are determined by considering the signs of the crack tip forces.

The kink angle Ω can be predicted by considering the mode mixity. It is known that a crack in a homogeneous isotropic material tends to propagate in the plane that is free from shear stress [17]. This leads to the following expression for the crack kink angle [18]:

$$(3.9) \quad \Omega = 2 \tan^{-1} \left[\frac{\sqrt{1 + 8 \left(\frac{K_{II}}{K_I} \right)^2} - 1}{4 \left(\frac{K_{II}}{K_I} \right)} \right],$$

where the definition of the crack kink angle Ω is shown in Fig. 10. The direction of this angle is defined in relation to the sign of the crack tip shear force defined in Fig. 9. A positive shear force causes the crack to kink downward, and a negative one causes it to kink upward.

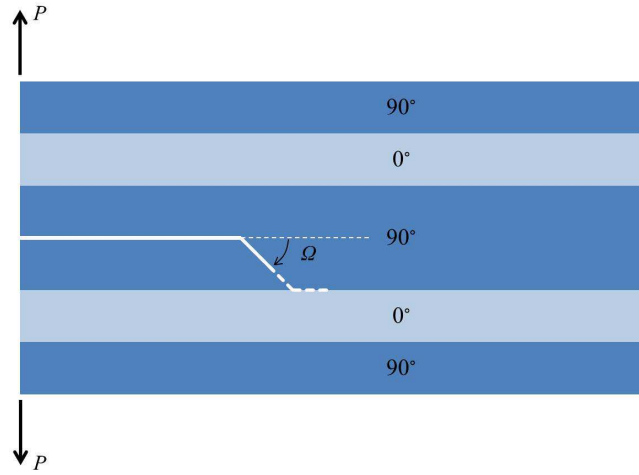


FIG. 10. Definition of crack kink angle.

When the thermal stresses are considered, the crack kink angle becomes a function of the load P , in which case another condition is necessary to determine the load. Hence, it is assumed that the crack propagates when the stress intensity factor $K_{\sigma, \max}$, which is induced by the tensile stress occurring on the plane in the direction of the kink angle, reaches the critical value of K_I , namely K_{IC} . At that time,

$$(3.10) \quad \begin{aligned} K_{\sigma, \max} &= \frac{1}{2} \left\{ K_I (1 + \cos \Omega) \cos \frac{\Omega}{2} + 3K_{II} \sin \Omega \cos \frac{\Omega}{2} \right\} \\ &= K_{IC} = \sqrt{E_T G_{IC}} \end{aligned}$$

is assumed to be satisfied. Practically, the kink angle can be found as follows. First K_I , K_{II} , and Ω are calculated by substituting a value into P . Then whether $K_{\sigma, \max}$ is larger than K_{IC} is evaluated. This procedure is repeated until $K_{\sigma, \max}$ just becomes larger than K_{IC} by increasing the value of P gradually from a small value. The last Ω is assumed to be the kink angle.

ERDOGAN and SIH [17] showed that a mixed-mode crack propagates at a larger external load than the maximum circumferential-stress criterion shown in (3.10). However, the experimental data are scattered over $\sim 30\%$ of K_{IC} . KAGEYAMA and OKAMURA [19] applied their proposed distributed dislocation method to determine the elastic field around an infinitesimal kink of a crack and used it to obtain a fracture criterion with respect to the energy release rate. This criterion was compared with the maximum circumferential-stress criterion and the minimum strain-energy-density criterion in the curves of fracture angle versus crack angle and of K_{II} versus K_I . The results showed that the former types of curves for the three criteria were in good agreement with each other. The latter type of curve for the maximum energy-release-rate criterion was in good agreement with the one for the maximum circumferential-stress criterion, but it differed slightly from the one for the minimum strain-energy-density criterion. However, the differences are within the experimental errors of [17]. Accordingly, the maximum circumferential-stress criterion is often used in practice because it is relatively simple, easy to understand, and easy to apply. Consequently, (3.9) was used also in this study.

3.2. Analytical results and discussion

The material properties used in the calculations are listed in Table 3. The thickness of one ply was assumed to be 0.26 mm. The cure temperature was assumed to be 130 °C.

Table 3. Material properties.

Symbol	Value
E_L [GPa]	118
E_T [GPa]	7.73
ν_{LT}	0.35
ν_{TT}	0.49
G_{LT} [GPa]	3.75
G_{TT} [GPa]	2.70
G_{IC} [J/m ²]	213
α_L [1/K]	0.156×10^{-6}
α_T [1/K]	59.6×10^{-6}

Two schematic crack-growth scenarios are shown in Fig. 11. It was assumed that an initial crack was located somewhere in the inner 90° layer. The normalized crack position refers to the ratio of h_{cp} to the thickness of the inner 90° layer. Hence, the normalized crack positions of the upper interface, center, and lower interface are 0, 0.5, and 1, respectively. Positive and negative kink angles denote that the crack kinked downward and upward, respectively. Accordingly, if the crack is located in the upper region and the crack kink angle is negative, the crack kinks upward, possibly reaches the $0^\circ/90^\circ$ interface, and tends to propagate along the interface because the crack is assumed not to be able to penetrate into the 0° layer, as shown by the red lines in Fig. 11a. However, if the crack is located in the upper region and the crack kink angle is positive, the crack kinks downward, possibly reaches the center of the specimen, and tends to propagate along the center or reach the $0^\circ/90^\circ$ interface beyond it, as shown by the blue lines in Fig. 11a. The paths assumed when the crack is located in the lower region are shown in Fig. 11b. The kink angle here is that of an infinitesimal kink from the tip of an initial horizontal crack. The subsequent kink angle cannot be predicted in this analysis. Accordingly, this angle cannot be compared directly with the measured ones listed in Table 1. The predicted kink angle at a normalized crack position of 0.5, i.e., at the center of the 90° layer, is indeed zero. Strictly speaking, this model is a form of static stability analysis and cannot be used to analyze the cracking behaviors after kinking. However, the tendency of the crack kinking can be estimated from the predicted results.

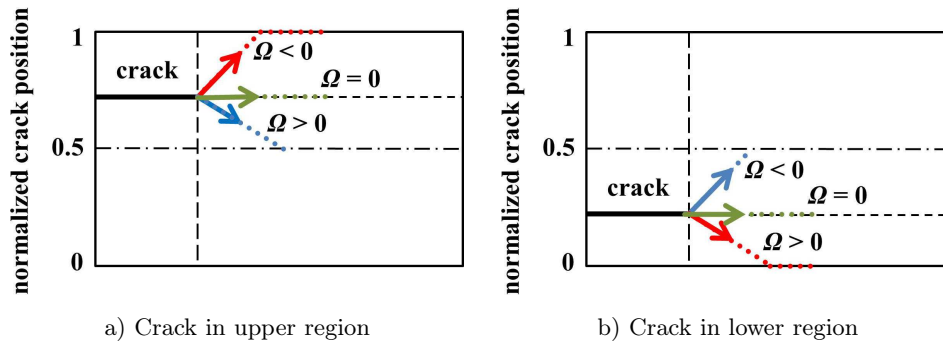
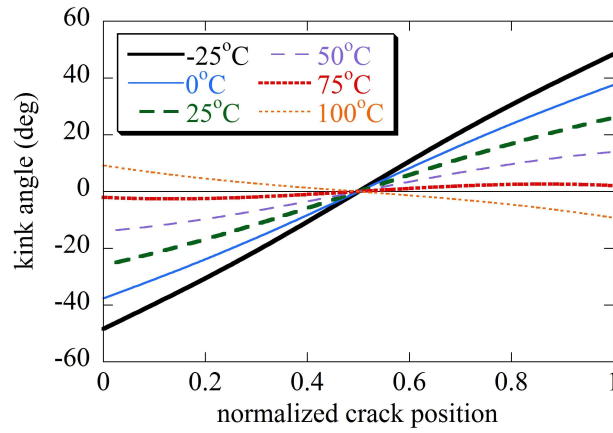
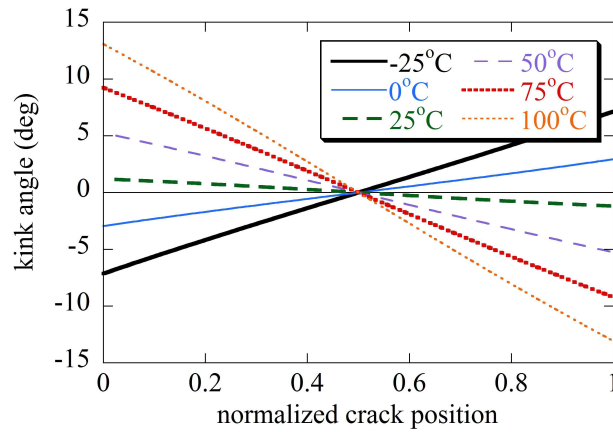


FIG. 11. Schematic crack-growth scenarios.

The crack kink angles calculated as a function of the crack position are shown in Fig. 12. For the Type A specimen at 100°C , the predicted kink angle is positive (negative) in the region between the upper (lower) $0^\circ/90^\circ$ interface and the center of the specimen. Accordingly, the crack tends to grow in a self-similar manner along the center of the specimen. This estimation agrees with the experimental observation that the propagating crack returned to the center even though it



a) Type A



b) Type B

FIG. 12. Predicted kink angle versus normalized crack position for 54 mm initial crack.

kinked briefly toward the interface. Such zigzag propagation will be discussed later. The predicted kink angles at $<75^{\circ}\text{C}$ are negative in the upper region and positive in the lower one. Accordingly, the cracks tend to propagate along one of the $0^{\circ}/90^{\circ}$ interfaces. This estimation also agrees with the experimental results. However, the crack jumped to the other interface after propagating a short distance along the interface at 75°C in the experiment. This behavior may have been caused by errors in the model and the material properties.

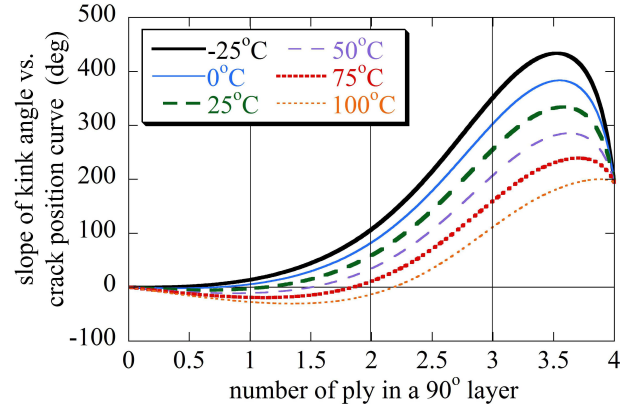
For Type B specimens at $>25^{\circ}\text{C}$, the predicted angles are positive in the upper region and negative in the lower one. Accordingly, the cracks tend to grow in a self-similar manner along the centers of the specimens. This estimation agrees with the experimental observations at 75°C and 100°C . Experimentally

at 25°C and 50°C, each of the cracks kinked and propagated to one of the 0°/90° interfaces, jumping to the other one after propagating a short distance along the first interface. We think that the reason for this phenomenon is that after a flexure fracture occurs and the crack reaches an interface, it then jumps to the other one because it tends to kink toward the center of the specimen. At -25°C and 0°C, the predicted angles are negative in the upper region and positive in the lower one. Accordingly, the cracks tend to propagate along 0°/90° interfaces, and this estimation also agrees with the experimental observations. However, as with the Type A propagation at 75°C, the crack jumped to the other interface in the experiment at 0°C.

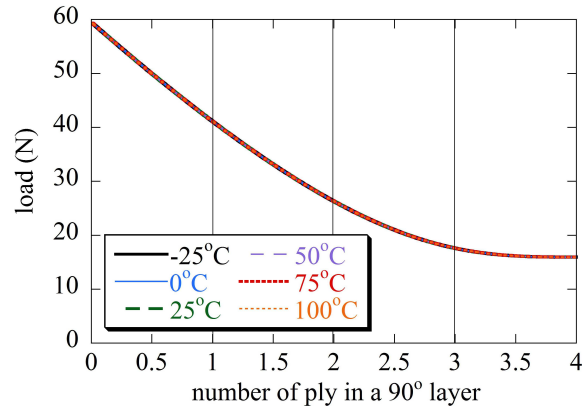
From Fig. 12, it can be seen that the crack kink angles in the upper region increase with temperature. Hence, the cracks tend to kink in general toward the centers of the specimens with increasing temperature; this trend agrees with the experimental results.

The dependencies of the number m of plies in a 90° layer on the rate of change of the kink angle with crack position and the applied load when the crack propagates along the center are shown in Fig. 13. In this study, the kink angle at $h_{cp} = 0.99h_{90}$ multiplied by 200 times was assumed to be the slope of the kink angle, and the applied load at $h_{cp} = 0.99h_{90}$ was assumed to be the load at the center since $\xi = 0$ and M_{1P} cannot be evaluated when $h_{cp} = h_{90}$. m was assumed to vary continuously in order to determine the tendency more easily, although in practice $m = 1, 2, 3$, or 4. When the slope is negative, a crack at the center tends to remain there as it propagates. It is assumed that the magnitude of the slope is related to the magnitude of the stability. The results indicate that a crack at the center propagates along the center more stably if the temperature is higher. Comparing Type A ($m = 2$) and Type B ($m = 1$), the latter is more stable. As m increases, the applied load decreases; this tendency is independent of temperature. It can be seen from the equations for M_{1P} and N_{1P} in (3.4) that the applied load is independent of temperature since $\alpha_{N2} = \alpha_{N1}$ and $\alpha_{M2} = \alpha_{M1} = 0$ at the center. The applied loads were 26 N for Type A ($m = 2$) and 41 N for Type B ($m = 1$). These tendencies agree well with the experimental results.

The predicted crack kink angles at the upper 0°/90° interface are listed in Table 4 for different crack lengths. It can be seen that the crack kink angles remain approximately constant even during interface crack propagation. However, the cracks sometimes jump to the other interfaces after propagating short distances along the 0°/90° interfaces in the experiments. Accordingly, this phenomenon cannot be explained by this analysis, because the analysis of the case in which the initial crack is on the upper interface is the same regardless of whether the crack was located there initially or came from the other location, although it is thought that the shear force at the crack tip induced by the difference between



a) Slope of kink angle versus crack position



b) Applied load

FIG. 13. Variations with number of plies in a 90° layer: a) slope of kink angle versus crack position curve; b) applied load when crack propagates along center.

the cure and the test temperature is different in the two cases. Hereafter, the shear force is referred to as the interlaminar shear stress.

To show the difference between the interlaminar shear stresses in the two cases, the stresses were calculated using commercial finite-element analysis (FEA) software (ANSYS ver. 16.1) for the two cases as shown in Fig. 14. In this analysis, the interlaminar shear stress at a distance of 0.1 mm from the crack tip was compared because the crack tip itself is a singular point. Although FEA is often used to predict crack propagation with sophisticated methods such as the VCCT and FNM [12], it was used here to predict only the stress distribution before the cracks started to propagate for the two different crack configurations. The jump phenomena occurring in the 90° layer will be discussed in relation to

Table 4. Predicted crack kink angles at upper interface for various crack lengths.

	Type	Temp. [°C]	Crack length			
			54 mm	56 mm	58 mm	60 mm
Predicted crack kink angle [°]	A	-25	-48.41	-48.39	-48.38	-48.37
		0	-37.59	-37.58	-37.56	-37.54
		25	-26.01	-25.99	-25.97	-25.95
		50	-14.00	-13.98	-13.96	-13.93
		75	-2.08	-2.06	-2.03	-2.01
		100	9.22	9.25	9.27	9.29
	B	-25	-7.14	-7.11	-7.08	-7.05
		0	-2.94	-2.91	-2.89	-2.86
		25	1.20	1.23	1.26	1.28
		50	5.26	5.29	5.32	5.34
		75	9.22	9.25	9.28	9.31
		100	13.07	13.10	13.13	13.15

this stress distribution. The case in which the crack located at the upper interface originated from the center was approximated by a crank-shaped model, as shown in Fig. 14b). The plane stress element PLANE183 (225,672 nodes, 73,735 elements for the straight crack with $l = 56.0$ mm) was used in the calculations. Here, l is defined as the length from the specimen edge to the initial crack tip, as shown in Fig. 14. Note that the numbers of nodes and elements required for different crack configurations and lengths differ slightly. The material properties used in this analysis are listed in Table 3; the thickness of one ply was assumed to be 0.26 mm. This numerical analysis was conducted for the Type B specimen at 25°C. The stress distribution due to the mechanical loads is considered to be almost the same for each configuration because of the equilibrium states of the forces and the moments. Therefore, we examined the stress distribution due to thermal loads alone. The interlaminar shear stress was calculated by changing the temperature from 130°C to 25°C.

The interlaminar shear stresses corresponding to different crack lengths l are given in Table 5. In the straight-crack case, this stress does not change even when the crack extends. However, in the case of a crank-shaped crack, the magnitude of the interlaminar shear stress decreases as the crack extends. Hence, the crack tends to kink toward one interface as it propagates along the other; this tendency is in good agreement with the experimental results.

Finally, the variations of the material constants with temperature should be discussed. The material constants of some types of resins depend strongly

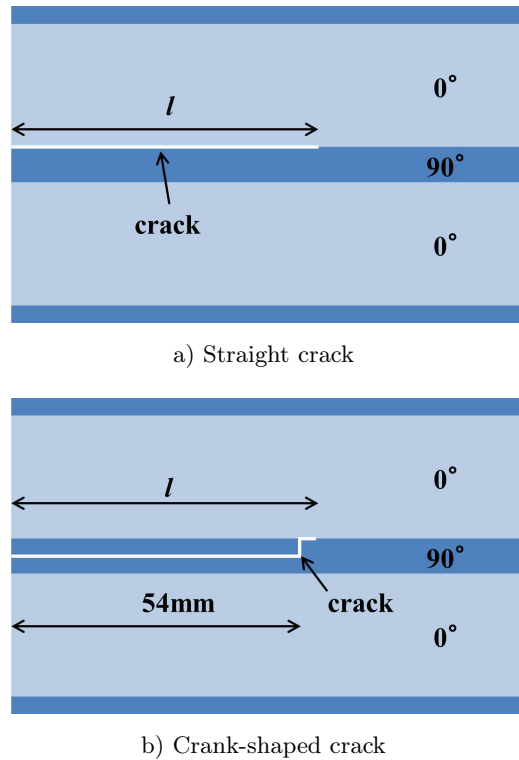


FIG. 14. Two crack cases for which interlaminar shear stress was calculated.

on temperature. The degree of this effect in the specimens used in this study was determined by inspecting the initial slopes of the load–displacement curves shown in Fig. 3. These are related directly to the bending rigidity. As shown in Fig. 3, Type A specimens seem to be affected more than Type B ones because the former have twice as many 90° plies, and, hence, their mechanical properties are affected more by the resin. However, the extent of this effect is assumed not to be significant to obtain a qualitative explanation from this simple analysis.

Table 5. Predicted interlaminar shear stresses induced by temperature difference in relation to crack length for Type B specimens at 25°C. These values presented were obtained at 0.1 mm from the crack tip.

l [mm]		54.5	55.0	55.5	56.0
Predicted interlaminar shear stresses [MPa]	Straight crack	−9.5	−9.5	−9.5	−9.5
	Crank-shaped crack	−16.8	−13.3	−11.6	−10.7

4. Conclusions

To understand the complex fracture behaviors of multidirectional laminates, especially cross-ply laminated plates, DCB tests of two types of cross-ply laminated plates with 90° layers in their centers were conducted at various temperatures. The crack propagation behaviors were then predicted analytically.

The load-displacement curves and crack propagation paths of the cross-ply laminates in the DCB tests were found to depend on the test temperature. As the temperature decreased, cracks tended to kink toward one of the $0^\circ/90^\circ$ interfaces and then propagate along the interfaces.

The energy release rates were calculated using the bi-layer shear-deformable beam model including residual thermal stress. The crack kink angles of the cross-ply laminated plates were predicted using these energy release rates. To solve the equations of the bi-layer shear-deformable beam model, an applied-load condition was introduced. The predictions showed that cracks at the centers of specimens would tend to propagate along their centers more stably at higher temperatures and in thinner 90° layers. As these layers became thicker, the applied load at which the cracks at the centers initiated propagation decreased, independent of temperature. These tendencies were in good agreement with the experimental results. Accordingly, this analysis is useful for predicting the general tendencies of crack propagation in cross-ply laminates.

However, the phenomenon of crack propagating a short distance along one interface and then jumping to the other one could not be explained. To investigate the reason for this behavior, the interlaminar shear stress after a crack jumped to the other interface and propagated along it was calculated using FEA. As a result, it was seen that the magnitude of the interlaminar shear stress decreased as the crack propagated, causing the crack to jump to the other interface after it had propagated a short distance along the first one.

References

1. D.L. HUNSTON, W.D. BASCOM, *Effects of lay-up, temperature, and loading rate in double cantilever beam tests of interlaminar crack growth*, Composites Technology Review, **5**, 4, 118–119, 1983.
2. P. ROBINSON, D.Q. SONG, *A modified DCB specimen for mode I testing of multi-directional laminates*, J. Composite materials, **26**, 11, 1554–1577, 1992.
3. H. CHAI, 1984, *The characterization of mode I delamination failure in non-woven multi-directional laminates*, Composites, **15**, 4, 277–290, 1984.
4. P. ROBINSON, F. JAVIDRAD, D. HITCHINGS, *Finite element modeling of delamination growth in the DCB and edge delaminated DCB specimens*, Composite Structure, **32**, 1–4, 275–285, 1995.

5. A.B. de MORAIS, M.F. de MOURA, J.P.M. GONCALVES, P.P. CAMANHO, *Analysis of crack propagation in double cantilever beam test of multidirectional laminates*, *Mechanics of Materials*, **35**, 7, 641–652, 2003.
6. T.A. SEBAEY, N. BLANCO, C.S. LOPES, J. COSTA, *Numerical investigation to prevent crack jump in double cantilever beam tests of multidirectional composite laminates*, *Composites Science and Technology*, **71**, 13, 1587–1592, 2011.
7. A.B. de MORAIS, M.F. de MOURA, A.T. MARQUES, P.T. CASTRO, *Mode-I interlaminar fracture of carbon/epoxy cross-ply composites*, *Composites Science and Technology*, **62**, 5, 679–686, 2002.
8. J.A. NAIRN, *Energy release rate analysis for adhesive and laminate double cantilever beam specimens emphasizing the effect of residual stresses*, *International Journal of Adhesion and Adhesives*, **20**, 1, 59–70, 2000.
9. J.G. RATCLIFFE, M.W. Czabaj, and T.K. O'BRIEN, *A test for characterizing delamination migration in carbon/epoxy tape laminates*, NASA/TM-2013-218028, 1–19, 2013.
10. J.G. RATCLIFFE and N.V. DE CARVALHO, *Investigating delamination migration in composite tape laminates*, NASA/TM-2014-218289, 1–19, 2014.
11. N.V. DE CARVALHO, B.Y. CHEN, S.T. PINHO, J.G. RATCLIFFE, P.M. BAIZ, and T.E. TAY, *Modeling delamination migration in cross-ply tape laminates*, *Composites: Part A*, **71**, 192–203, 2015.
12. M.F. PERINCE, N.V. DE CARVALHO, J.G. RATCLIFFE, P.M. BAIZ, and S.R. HALLETT, *Experimental study on delamination migration in composite laminates*, *Composites: Part A*, **73**, 20–34, 2015.
13. L.A. CARLSSON, R.C. MATTESON, F. AVILES, D.C. LOUP, *Crack path in foam cored DCB sandwich fracture specimens*, *Composites Science and Technology*, **65**, 15–16, 2612–2621, 2005.
14. T. YOKOZEKI, *Analysis of crack kinking in foam core sandwich beams*, *Composites Part A*, **42**, 10, 1493–1499, 2011.
15. JAPANESE INDUSTRIAL STANDARDS, *Testing method for interlaminar fracture toughness of carbon fibre reinforced plastics*, JIS K7086-93, Japanese Standards Association, Tokyo, 1998.
16. T. YOKOZEKI, *Energy release rates of bi-material interface crack including residual thermal stresses: application of crack tip element method*, *Engineering Fracture Mechanics*, **77**, 1, 84–93, 2010.
17. F. ERDOGAN, G.C. SIH, *On the crack extension in plates under plane loading and transverse shear*, *Journal of Basic Engineering*, **85**, 4, 519–527, 1963.
18. S. PRASAD, L.A. CARLSSON, *Debonding and crack kinking in foam core sandwich beam-I. Analysis of fracture specimens*, *Engineering Fracture Mechanics*, **47**, 6, 813–824, 1994.
19. K. KAGEYAMA, H. OKAMURA, *Elastic Analysis of Infinitesimally Kinked Crack under Tension and Transverse Shear and the Maximum Energy Release Rate Criterion*, *Transactions of the Japan Society of Mechanical Engineers Series A*, **48**, 430, 783–791, 1982 [in Japanese].

Received November 1, 2015; revised version August 17, 2016.

